Check for updates

Received: 29 November 2019 | Revised: 3 February 2020 | Accepted: 11 February 2020

DOI: 10.1002/mds3.10071

RAPID COMMUNICATION

MEDICAL DEVICES & SENSORS WILEY

A pathogen imprinted hybrid polymer capacitive sensor for selective *Escherichia coli* detection

Samuel M. Mugo[1] | Weihao Lu[1] | Dhanjai Dhanjai[1,2]

[1]Physical Sciences Department, MacEwan University, Edmonton, AB, Canada

[2]Department of Mathematical and Physical Sciences, Concordia University of Edmonton, Edmonton, AB, Canada

Correspondence
Samuel M. Mugo, Physical Sciences Department, MacEwan University, 10700-104 Avenue, Edmonton, AB T5J 4S2, Canada.
Email: mugos@macewan.ca

Funding information
Natural Sciences and Engineering Research Council of Canada; Macewan University Research Office

Abstract

A versatile pathogen imprinted polymer electrochemical sensor has been developed for *Escherichia coli* detection. The sensor is based on layer by layer assembly of multi-walled carbon nanotubes (CNT), nanocellulose (CNC) films, integrated with polyaniline (PANI) doped phenylboronic acid (PBA). The sensing layer is a poly(methacrylic acid) based pathogen microcontact imprinted polymer (PIP). The PIP@PBA/PANI@CNT/CNC sensor exhibits a high affinity towards *E. coli* in real biological matrices, while effective in discriminating *E. coli* amidst other bacteria. Using capacitance and impedance as transduction methods, the PIP sensor recorded a low limit of *E. coli* detection of 8.7 ± 0.5 cfu/ml, with a rapid response of ≤5 min.

KEYWORDS

cell imprinted polymers, *E. coli* capacitive sensor, pathogen imprinted polymers

1 | INTRODUCTION

Food and drinking water contamination from bacterial pathogens is a global public health concern (Blount, 2015; Health Canada, 2013a, 2013b). Food-borne disease outbreaks are prevalent in countries in the Global South and common in the Global North countries (Blount, 2015; Health Canada, 2013a, 2013b). The most common outbreaks reported are attributed to bacterial strains such as *E. coli*, *Giardia*, *Cryptosporidium*, *Helicobacter pylori*, *Campylobacter* and *Salmonella*. Of these diarrhoeal virulent bacteria, *E. coli* (e.g. *E. coli* O157:H7) contamination in foods and water is highly prevalent. Naturally present in digestive tracts of warm-blooded animals, *E. coli* is used as a definitive indicator of faecal contamination in drinking and recreation water (Wu et al., 2012). As such, rapid tools for *E. coli* detection are of societal relevance.

Conventional techniques used for *E. coli* detection include microscopy, immunoassays and quantitative polymerase chain reaction (*qPCR*), ATP bioluminescence, flow cytometry and solid-phase cytometry-based techniques. These analytical methods require laboratory-localized expensive instruments that demand tedious sample preparation and skilled professional for operation. The common microbial culturing and colony counting detection method takes at least 3 days for sample analysis (Blount, 2015; Mandal, Biswas, Choi, & Pal, 2011; Wu et al., 2012). Such a delay could compromise public safety in cases of outbreaks. The lack of rapid and cost-effective quantitative microbial detection tools constrains food and water quality monitoring (Zhao et al., 2016). Thus, economical, fast and on-field analytical tools are necessary. Due to their low cost, ease of miniaturization, and minimal sample pre-treatment, there is growing interest in electrochemical sensors for food-borne pathogens detection. Inherent in the electrochemical sensors are electrodes that integrate biological receptors, for example aptamers, antibodies and enzymes, that selectively capture the pathogen, an interaction that induces a measurable change in electrode electrical properties (Ahmed, Rushworth, Wright, & Millner, 2013; Isık et al., 2017; Liu, Settu, Tsai, & Chen, 2015). (Bio)chemical sensors comprising integration of these biological receptors to different nanomaterials, including gold, copper, silica, graphene and carbon nanotubes, have been explored with promising results to analytical platforms for point-of-care/use diagnostic systems (Brosel-Oliu, Abramova, Uria, & Bratov, 2019; Butina, Loffler, Rhen, & Richter-Dahlfors, 2019; Gupta, Bhardwaj, Sharma, Kim, & Deep, 2019; Ma et al., 2008). The challenge with biological receptors is their cost, thermochemical instability and reusability. In contrast, pathogen imprinted polymers (PIP) are versatile, selective, thermo-chemically stable synthetic biomimetic molecular receptors (Idil, Hedstrom, Denizli, & Mattiasson, 2017; Shen et al., 2014). The PIP are synthesized by copolymerization of appropriate monomers,

 © 2020 Wiley Periodicals, Inc.

crosslinkers and the pathogen template. Upon removal of the pathogen, cavities that bear structural similarity and size to the removed pathogen template prevail in the polymer network (Idil et al., 2017).

Herewith, we demonstrate a PIP-based electrochemical capacitive sensors for detection of *E. coli* K-12. Briefly, the electrochemical sensor is built by layer by layer (LbL) assembly. The layers are comprised of (a) polyvinyl acetate sheet; (b) multi-walled carbon nanotube/cellulose nanocrystal (CNC/CNT) nanoporous conductive film coated with polyaniline (PANI) doped with phenylboronic acid (PBA) and (c) poly(methacrylic acid) as the *E. coli* K-12 PIP. The sensor PIP affinity capture of *E. coli* changes the electrical properties (capacitance and impedance) of the sensor film electrode.

2 | EXPERIMENTAL

2.1 | Chemicals and reagents

All aqueous solutions were prepared using >18 MW Milli-Q water (Millipore). The multi-walled carboxylic acid-functionalized carbon nanotubes (CNT) (diameter 9.5 nm × 1.5 μm), cyclohexanol, lysozyme, glycidyl methacrylate (GMA), ethylene glycol dimethacrylate (EGDMA), 4,4′-azobis(4-cyanovaleric acid) (ACVA), 3-(2-carboxyethyl) boronic acid (PBA), aniline, Tris-buffer and ammonium persulfate were purchased from Sigma-Aldrich Co. The Lysogeny broth (LB) and agar, Tris base, were supplied by Thermo Fisher Scientific. The *E. coli* K-12, *Bacillus cereus* and *Staphylococcus aureus* strains were obtained from the Department of Biology, MacEwan University. The cellulose nanocrystals (CNC) were donated by Alberta Innovates. The polyvinyl acetate (PVA) transparency sheets were obtained from a local stationery store.

2.2 | *E. coli* stamp preparation

The *E. coli* stock solution was prepared by incubating a culture of *E. coli* K-12 in 150 ml Lysogeny broth in a 37°C shaker (at 150 rpm) for 24 hr. The *E. coli* concentrate solution was then centrifuged at 2683 *g* for 20 min and washed three times with 0.1 M KCl. The bacterial count (cfu/ml) in the *E. coli* concentrate was estimated by standard plate count method. To prepare the *E. coli* stamp, a PVA sheet (1.5 × 1.5 cm^2) was sonicated in 1.0 M H_2SO_4 for 10 min, rinsed with deionised water, with 1.0 M NaOH and finally with 70% ethanol. A 50 μl of *E. coli* suspension was drop casted onto the clean PVA sheet and allowed to dry in an enclosed incubator. The resultant *E. coli* stamps were stored at 4°C until use.

2.3 | Fabrication of the nanoporous conductive film

A 100.0 μl of 1.0 mg/ml CNT/CNC (1:1 *wt/wt*) aqueous nanocomposite suspension was drop casted on a PVA sheet (1.5 cm^2) and dried for ~1 hr resulting in a conductive film of 0.5 cm radius.

A 50 μl solution comprising 750 μl of 0.1 M aniline in 0.5 M H_2SO_4, 250 μl of 0.1 M [3-(2-carboxyethyl)phenyl]boronic acid (PBA) and 100 μl of 0.05 M ammonium persulfate was drop casted the CNT/CNC film. The PBA/PANI polymerization ensued at 4°C for 5 hr. To evaluate the optimal thickness and surface distribution of the PBA/PANI on the sensor, the aniline/PBA polymerization step was repeated up to three times with the electrochemical performance of the films tested after each polymerization event (Dhanjai, Yu, & Mugo, 2019).

2.4 | Preparation of PIP *E. coli* sensor

The *E. coli* PIP layer was coated on PBA/PANI@CNT/CNC film using surface microcontact polymerization technique. A 50 μl prepolymer mixture comprising—GMA monomer (26 μl), EGDMA crosslinker (80 μl), ACVA radical initiator (2.0 mg) and cyclohexanol porogenic solvent (400.0 μl)—was added to the PBA/PANI@CNT/CNC film. The PVA *E. coli* stamp (described above) was brought into contact with the prepolymer aliquot, and then polymerization initiated by UV radiation (18 W, 312 nm) for 3 hr. The PIP@PBA/PANI@CNT/CNC sensor film was then washed with 0.1 M phosphate buffer (pH = 7.2) to rinse off unbound prepolymer and to ease *E. coli* stamp removal. The film was further treated with 200.0 μl lysozyme buffer (10.0 mg/ml lysozyme in 10.0 mM Tris-buffer, pH 7.0) for 30 min to digest the *E. coli* cells, removing them from the imprinted polymer network. Following *E. coli* template removal, the sensor film was washed off using deionised water. As a control, a non-imprinted imprinted polymers (NIP) form (control) of the sensor was prepared through the same procedure, but a PVA sheet devoid of *E. coli* was used as the stamp. The developed PIP-based sensor morphology was characterized using Zeiss Sigma Field Emission scanning electron microscopy (FE-SEM) and evaluated for *E. coli* capture by electrochemical analysis. The fabricated PIP@PBA/PANI@CNT/CNC *E. coli* sensor is depicted in Figure 1.

2.5 | Electrochemical analysis of the PIP *E. coli* sensor

The PIP@PBA/PANI@CNT/CNC sensor was evaluated for detection of *E. coli* by analysis with cyclic voltammetry (CV), acquired at a range of −0.95 to +0.95V at a scan rate of 0.10 V/s. The CV was acquired using Palmsens 4 potentiostat with PSTrace software (PalmSens BV). The PalmSens potentiostat used has Bluetooth capability and a smartphone software app. A smartphone was used as the interface for capacitive data acquisition. The use of smartphone depicted in Figure 1 emphasizes the portability of the *E. coli* sensor. The capacitance signal as a function of *E. coli* concentration (0–6.22 × 10^6 cfu/ml) was determined. Capacitance was determined from the cyclic voltammograms by taking a ratio of current to scan rate. The three-electrode system for CV acquisition comprised the PIP@PBA/PANI@CNT/CNC sensor (or control NIP sensor) as

working electrode, platinum as the auxiliary electrode, and an in-house fabricated Ag/AgCl reference electrode (Dhanjai et al., 2019).

The impedance measurements were performed using the on the PIP sensor using the same set-up and voltage settings, with operating frequency fixed at 60 Hz. As with CV, the PalmSens 4 potentiostat and PS Trace software were used for impedance.

A 50 µl of 0.1 M phosphate buffer (pH 7.0) was deposited on the sensor and the blank cyclic voltammogram acquired. After the blank, 50 µl of different *E. coli* standards was exposed to the PIP-based sensor. Before acquiring the cyclic voltammograms, a 5 min residence time was allowed for molecular interactions between the polymer and the *E. coli* to ensue. The sensor was then rinsed three times with 0.1 M phosphate buffer (pH 7.0), and then, a cyclic voltammogram was acquired on a drop of 0.1 M phosphate buffer as an electrolyte. Each of the *E. coli* standard was analysed in triplicate after every addition. To determine the PIP-based sensor response to interfering pathogen species, the sensor response to Gram-positive bacteria, *S. aureus* and *B. cereus* in presence and without *E. coli* was evaluated. The *E. coli* PIP@PBA/PANI@CNT/CNC sensor was also evaluated for its detection of *E. coli* spiked in orange juice (Minute Maid® premium original), to simulate a real-life sample.

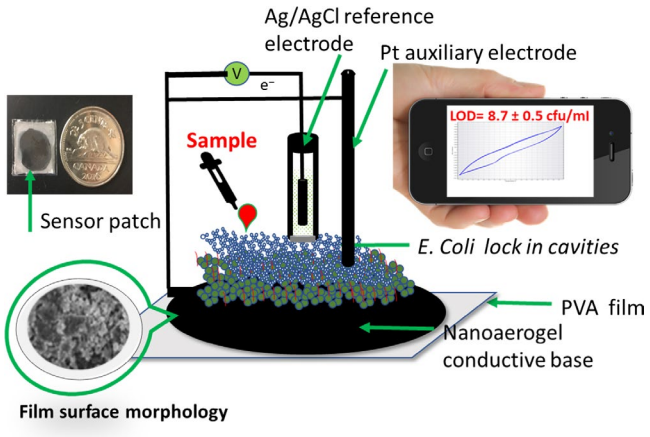

FIGURE 1 Scheme of the PIP@PBA/PANI@CNT/CNC *Escherichia coli* sensor, depicting the prevailing LbL components

3 | RESULTS AND DISCUSSION

3.1 | Structural characterization of fabricated PIP sensor

As depicted in Figure 1, the *E. coli* sensor comprises the PIP coated on a CNT/CNC that is printed on a PVA sheet. The CNT/CNC nanoporous film provides the conductive features borne from the high electromechanical properties of the CNT. The CNT used had carboxylic acid groups which interact with the surface hydroxyl groups of the CNC through intra-chain hydrogen bonding, thus leading to formation of stable nanoporous film electrode that affords excellent water absorbency due to the hydrogel nature of the CNC (Alzaid et al., 2017; Nemoto, Saito, Isogai, & Isogai, 2015; Plawsky, Kim, & Schubert, 2009). The CNC/CNT film porous fibrillar nanostructures (~20–200 nm) are evident in the SEM shown in Figure 2a. Ghaemi et al. (2018) have characterized similar CNC/CNT composite films by Brunauer–Emmett–Teller (BET), indicating a high surface area in the

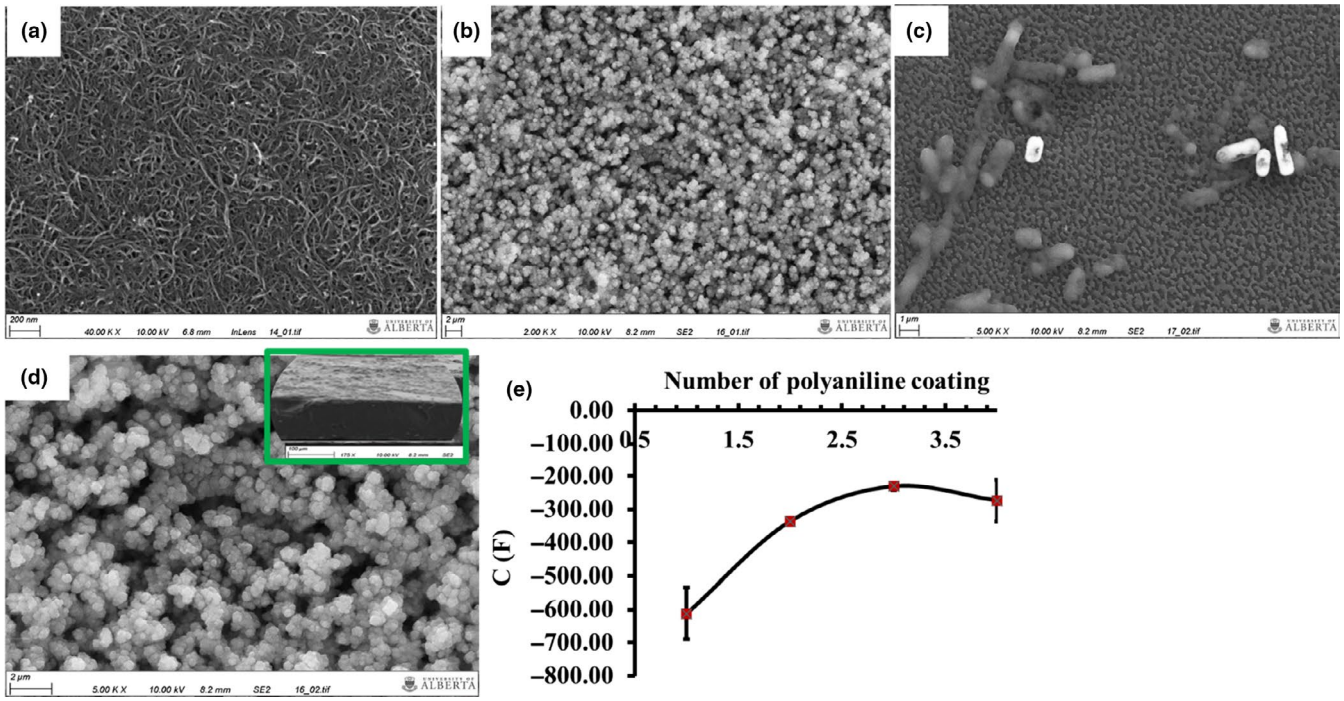

FIGURE 2 SEM images of (a) CNT/CNC, (b) PBA/PANI@CNT/CNC film, (c) *Escherichia coli* colony on a PVA sheet used as a stamp, (d) *E. coli* PIP@PBA/PANI@CNT/CNC film after lysis by lysozyme and (e) capacitance change with PANI coating layer on the CNT/CNC film

range of 15.2–21.1 m^2/g. The PBA/PANI was further coated onto the CNT/CNC to increase the film conductivity, while also improving the film stability (Golabi et al., 2016). In addition, boronic acid groups are known to interact with cis-diol functional groups to form cyclic esters. The Gram-negative bacteria have an outer membrane comprising lipopolysaccharides with cis-diol groups that interact with boronic acid (Li, Zhu, Marken, & James, 2015; Zhang et al., 2017). PBA was integrated into the conductive aerogel film as one of the selective molecular probes to capture the *E. coli*. As shown in Figure 2b, the PANI/PBA thinly encapsulates and fills the interstices of the CNC/CNT conductive layer.

To further improve the *E. coli* sensor selectivity, a thin film of PIP based on polymethacrylate was further coated to the PBA/PANI@CNT/CNC film using an *E. coli* bacteria imprint stamp, shown in Figure 2c. Following polymerization and lysis of bacteria by lysozyme, *E. coli* imprint cavities are left on the PIP. Both the PIP and the PBA work synergistically as molecular receptors to offer a high selectivity to the *E. coli* bacteria (Li et al., 2015). The surface morphology of the imprinted polymer is shown in Figure 2d, with evidence of microporosity similar in shape to the rod-shaped *E. coli* template. The multilayer thickness of the PIP@PBA/PANI@CNT/CNC film is estimated to be ~50 μm, as shown by cross-section insert SEM image in Figure 2d.

The conductivity of the PBA/PANI@CNT/CNC film was significantly impacted by the amount of PANI/PBA coating. We determined the optimal coating cycles by repeating the in situ PBA/PANI polymerization step on CNT/CNC film multiple times. The resulting films were characterized by cyclic voltammetry, with capacitance measured by taking the ratio of the average cathodic current (potential window is from 0 to −0.2 V) with scan rate. As evident in Figure 2e, the capacitance of the PBA/PANI@CNT/CNC film increased up to the polymerization coating cycle. All the sensors were fabricated by three PBA/PANI polymerization coating cycles.

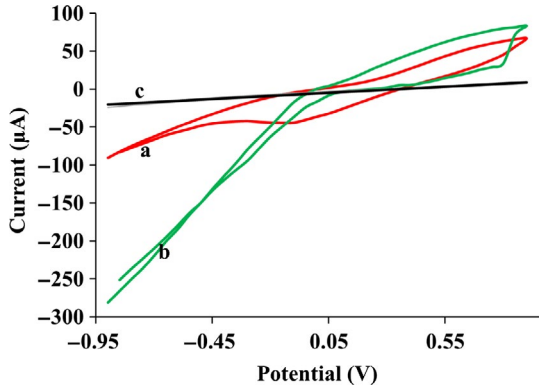

FIGURE 3 Cyclic voltammogram for 5 mmol $K_3[Fe(CN)_6]$ in 0.1 M KCl with (a) CNT/CNC, (b) PBA/PANI@CNT/CNC and (c) PIP@PBA/PANI@CNT/CNC film electrodes

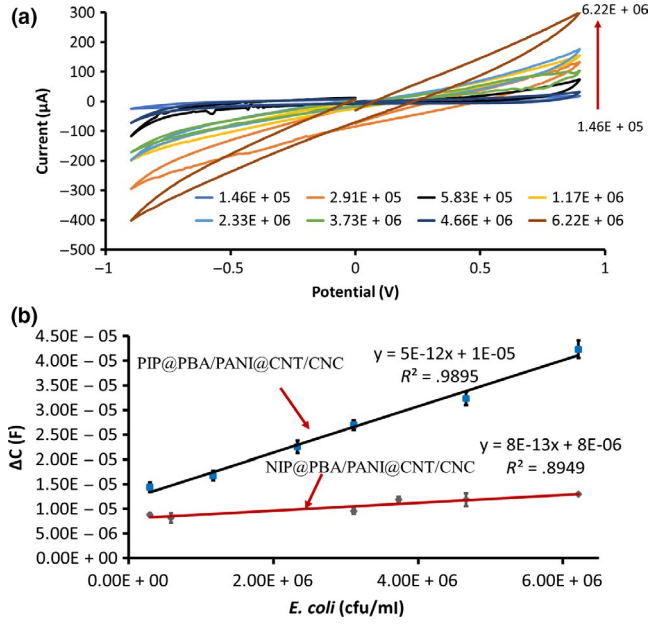

FIGURE 4 (a) Cyclic voltammograms obtained for PIP@PBA/PANI@CNT/CNC sensor with detection of *Escherichia coli*; (b) calibration plot of Δcapacitance (F) as a function of *E. coli* for PIP@PBA/PANI@CNT/CNC and NIP@PBA/PANI@CNT/CNC sensors

3.2 | Electrochemical characterization

The PIP@PBA/PANI@CNT/CNC sensor was characterized by cyclic voltammetric studies after fabrication of each coating layer. The CNT/CNC, PBA/PANI@CNT/CNC and PIP@PBA/PANI@CNT/CNC electrodes were analysed for their cyclic voltammetric response on 5 mmol $K_3[Fe(CN)_6]$ containing 0.1 M KCl as standard redox probe. As shown in the overlapped voltammogram in Figure 3a, the CNT/CNC film electrode has a well defined cathodic and anodic curve, indicative of excellent conductivity. As shown in Figure 3b, a higher cathodic and anodic response was observed after integration of PBA/PANI to the CNT/CNC, attributed to the inherent electroactivity of PANI due to electron delocalized π bonds (Zhang et al., 2017). However, following *E. coli* PIP coating, the electroactivity of the PIP@PBA/PANI@CNT/CNC (Figure 3c) was lower, due to the resistance of the PIP polymethacrylate polymer.

3.3 | Electrochemical detection of *E. coli* on the PIP@PBA/PANI@CNT/CNC electrode

The PIP@PBA/PANI@CNT/CNC sensor was tested for detection of *E. coli* standards with data acquisition performed by cyclic voltammetry. Figure 4a shows a representative overlapped cyclic voltammogram obtained for PIP@PBA/PANI@CNT/CNC sensor with detection of *E. coli* at different standard concentrations. Calibration regression was obtained by calculating the change in capacitance of the average cathodic current peak of the cyclic voltammogram for the sample compared to the blank. The average cathodic capacitance used as the sensor signal was determined by taking the ratio of the average of current density in the 0 to −0.2 V potential range with the scan rate (0.1 V/s). Figure 4b shows the excellent Δcapacitance

linear response as a function of *E. coli* for the PIP@PBA/PANI@CNT/CNC sensor and the non-imprinted polymer version (NIP@PBA/PANI@CNT/CNC). The PIP sensor was an order of magnitude more sensitive compared to the NIP version, as evident in the calibration sensitivity in Figure 4b. The limits of detection (LOD) of PIP@PBA/PANI@CNT/CNC sensor compared to NIP@PBA/PANI@CNT/CNC sensor was calculated to be 8.7 ± 0.5 and 78.7 ± 0.3 cfu/ml, respectively. These values were determined from triplicate measurements. The LOD was determined by taking the ratio of three times standard deviation of the phosphate buffer blank with calibration sensitivity (slope).

To evaluate the utility of each film component to the *E. coli* performance, different sensor film types were further evaluated for *E. coli* detection using cyclic voltammetry, and the linear regression for each determined. Table 1 summarizes the linear regression equations for the different variations of the sensor films. It is evident that the best performing sensor was PIP@PBA/PANI@CNT/CNC sensor, which integrated the synergy of *E. coli* cell wall affinity to PBA and the PIP selective cavities. The PIP@PANI@CNT/CNC film (no PBA) also showed a good response, but with an LOD of 19.7 ± 0.7 cfu/ml, indicating inclusion of PBA significantly improves the sensitivity of the sensor. The PIP@CNT/CNC (no PBA/PANI layer) had a LOD of 48 ± 1 cfu/ml, which while impressive, the results demonstrate the performance enhancement is increased from inclusion of the PBA/PANI layer. The PIP@CNT/CNC film on the other hand had a much lower LOD at 393 ± 10 cfu/ml, due to the absence of the cellular affinity receptors within the polymer matrix. Compared to the other methods of *E. coli* detection (Table 2), the LOD value obtained from this study is the lowest value in literature (Ajish et al., 2018; Idil et al., 2017; Li & Kosel, 2014; Poller, Spieker, Lieberzeit, & Preininger, 2017; Rengaraj, Cruz-Izquierdo, Scott, & Di Lorenzo, 2018; Zhang et al., 2018). The legislated maximum *E. coli* levels in foods, drinking water and recreational water vary from jurisdictions. In Canada, the maximum allowable *E. coli* levels in drinking water are 0 CFU/100 ml Health Canada, 2013a, 2013b). In swimming water, the accepted *E. coli* is ≤400 CFU/100 ml (Health Canada, 2013a, 2013b). As such, the sensor LOD is only slightly higher than the acceptable limit in food and drinks, and can be used as a rapid screening tool. The sensor would, however, be effective for screening and detection in recreational water in beaches, swimming pools and wastewater treatment plants before discharge.

3.4 | Probing the PIP *E. coli* sensor by impedance

The electrochemical performance of the PIP *E. coli* sensor was evaluated by impedance spectroscopy. Impedance is a powerful tool for investigating the subtle electrical changes of a conductive material following chemical perturbation. As with CV, the PalmSens 4 potentiostat and PS Trace software were used to determine impedance. At fixed frequency, 60 Hz, impedance curve fitting was not necessary, and a single impedance value from the sensor was obtained. Figure 5 shows the calibration curve obtained for PIP@PBA/PANI@CNT/CNC and NIP@PBA/PANI@CNT/CNC sensors. The impedance for the PIP@PBA/PANI@CNT/CNC sensors significantly decreases with increase of the *E. coli* concentration. The PIP sensor was ~18 times more sensitive than the NIP form, indicative of the specificity impacted by imprinting. However, the linearity of the calibration was not as ideal, compared to the cyclic voltammetry transduction approach. The calculated LOD for the PIP@PBA/PANI@CNT/CNC sensor was determined to be 2.62×10^7 cfu/ml, comparable to bacterial quartz-crystal microbalance sensors (Li et al., 2015). Impedance spectroscopy can be affected by numerous electrical parameters, and as such require finer control. Improvements for our detection system by impedance may be necessary to achieve LOD comparable or better than the capacitance results reported above.

TABLE 1 The summary of all the sensors used in Δcapacitance test

Sensor film types	Linear regression equation	LOD (cfu/ml)
PIP@CNT/CNC	$y = 8 \times 10^{-8}x - 0.086$ ($r^2 = .83$)	48 ± 1
PIP@PANI@CNT/CNC	$y = 4 \times 10^{-7}x - 1.2539$ ($r^2 = .79$)	19.7 ± 0.7
PIP@PBA/PANI@CNT/CNC	$y = 9 \times 10^{-7}x + 3.6111$ ($r^2 = .98$)	8.7 ± 0.5
NIP@CNT/CNC	$y = 2 \times 10^{-8}x - 0.6282$ ($r^2 = .87$)	390 ± 10
NIP@PBA/PANI@CNT/CNC	$y = 1 \times 10^{-7}x + 5.1688$ ($r^2 = .89$)	78.7 ± 0.3

TABLE 2 Comparison of different methods for *E. coli* detection

Methodology for *E. coli* target	LOD, cfu/ml
AIE (Aggregation-induced emission)-based glycoacrylamides fluorescent sensor (Ajish et al., 2018)	7.30×10^5
Magneto-resistive biosensors with an electromagnetic trap (Li & Kosel, 2014)	6.6×10^6
Biorecognition element based impedimetric sensor (Rengaraj et al., 2018)	1.93×10^3
Lipopolysaccharide based aptasensor (Zhang et al., 2018)	10^2
Whole cell-based microcontact imprinted capacitive biosensor (Idil et al., 2017)	70
Bacterial Quartz-Crystal Microbalance Sensors (Poller et al., 2017)	1.4×10^7
This work	8.7 ± 0.5

3.5 | Specificity of the *E. coli* PIP sensor

The PIP@PBA/PANI@CNT/CNC sensor was evaluated for its specificity and ability to differentiate *E. coli* amidst a matrix of other food-borne pathogens namely *S. aureus* and *B. cereus*. *S. aureus* is a round-shaped bacteria with diameters of 0.5–1.5 μm (Harris, Foster, & Richards, 2002). Both *E. coli* and *B. cereus* are rod shaped. The *B. cereus* is larger in size than *E. coli*. It is hypothesized with the PIP selective in size and shape to the *E. coli* pathogen imprint, the sensor should have preferential affinity to *E. coli*. Moreover, *B. cereus* and *S. aureus* are Gram-positive bacteria and are in general devoid of the lipopolysaccharide, the specific binding target for the PBA that is integrated in the sensor. The lipopolysaccharide is a chemical signature of Gram-negative bacteria cell walls (Zhang et al., 2018). Figure 6a shows the overlapped voltammograms, while Figure 6b depicts the bar graph of the Δcapacitance PIP sensor response to different combinations of bacteria samples, including (i) *E. coli* only, (ii) *B. cereus* only, (iii) *S. aureus* only, (iv) *E. coli* and *B. cereus*, (v) *E. coli* and *S. aureus*, and (vi) *E. coli*, *B. cereus* and *S. aureus*. The concentration of the *E. coli*, *B. cereus* and *S. aureus* in the analysed samples was 4.79×10^7, 8.10×10^6 and 4.77×10^7 cfu/ml, respectively. As shown in Figure 6b, the sensor had negligible response to *S. aureus*, attributed to the its difference in shape and cell wall structure. The PIP sensor showed some response to *B. cereus* due to its similarity in shape to *E. coli*. However, the PIP sensor was an order of magnitude more responsive to *E. coli* compared to *B. cereus*, indicative of preferential selectivity to *E. coli*. Similarly shown in Figure 6b, spiking *E. coli* to these Gram-positive bacteria, resulted in a significant spike in response, attesting to the sensitivity of the sensor to *E. coli*. As such, the PIP@PBA/PANI@CNT/CNC sensor can differentiate *E. coli* from *S. aureus and B. cereus* as Gram-positive species.

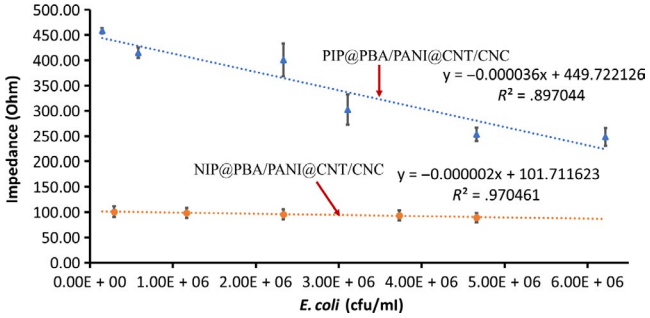

FIGURE 5 Calibration plot of impedance as a function of *Escherichia coli* for PIP@PBA/PANI@CNT/CNC and NIP@PBA/PANI@CNT/CNC sensors

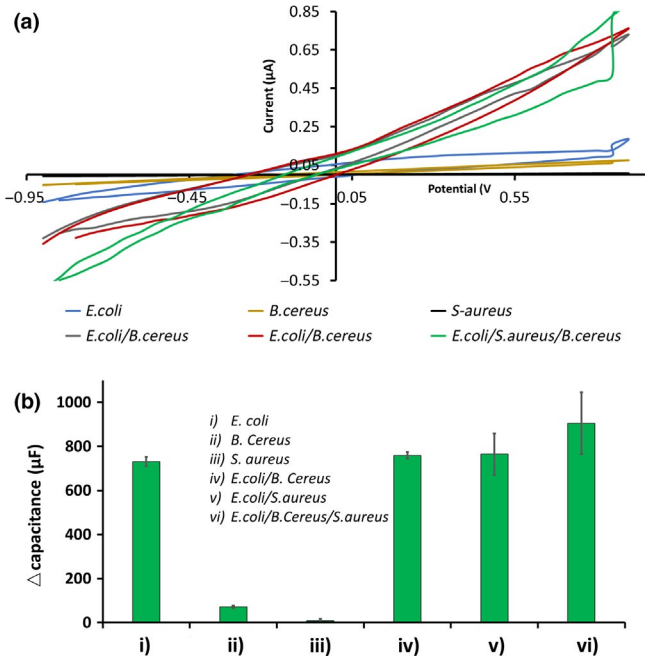

FIGURE 6 (a) Overlapped cyclic voltammogram comparing the PIP@PBA/PANI@CNT/CNC sensor response to different pathogen: (i) *Escherichia coli* only, (ii) *Bacillus cereus* only, (iii) *Staphylococcus aureus* only, (iv) *E. coli* and *B. cereus*, (v) *E. coli* and *S. aureus* and (vi) *E. coli*, *B. cereus*, *S. aureus* and *E. coli*. The amount of *E. coli*, *B. cereus* and *S. aureus* in each group is 4.79×10^7, 8.10×10^6 and 4.77×10^7 cfu/ml, respectively. (b) A bar graph showing the PIP sensor capacitance response as a function of the different pathogens

3.6 | Spiked juice sample application

The utility of the PIP@PBA/PANI@CNT/CNC sensor in detection of *E. coli* in a simulated real sample was evaluated. Neat commercial orange juice was analysed by the sensor and subsequently spiked with 3.84×10^6 and 9.6×10^6 cfu/ml *E. coli* standard. As shown in overlapped cyclic voltammogram in Figure 7, the PIP sensor responded to standard addition of *E. coli* to the juice sample. The inset bar graph in Figure 7 shows the capacitance linear increase with each additional *E. coli* standard spike. As such, it is evident the high sensitivity of the developed PIP sensor for detection of *E. coli* in a real beverage sample.

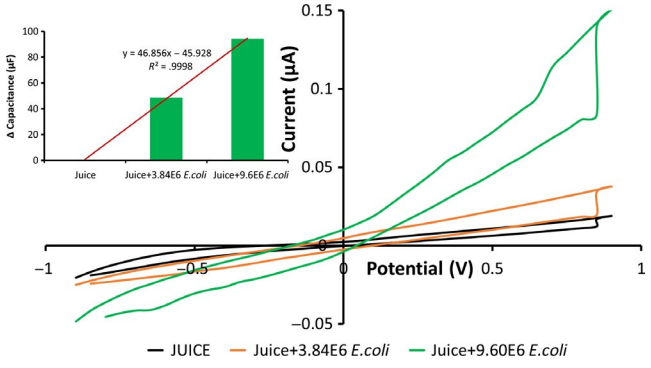

FIGURE 7 An overlapped voltammogram showing the PIP sensor response to juice sample in neat form and spiked with different concentrations of *Escherichia coli*. The figure also shows an inset of the corresponding capacitance response as a function of the *E. coli* spikes in juice

4 | CONCLUSION

An *E. coli* imprinted based sensor has been demonstrated. The developed PIP@PBA/PANI@CNT/CNC sensor is selective for *E. coli* detection in spiked simulated real samples, demonstrated in an orange juice sample in this paper. Based on size and shape of the bacteria, the *E. coli* sensor was effective in discriminating between different Gram-negative from Gram-positive bacteria. In this paper, it was demonstrated the PIP sensor was virtually unresponsive to the round-shaped Gram-positive bacteria *S. aureus* and was only marginally responsive to the rod-shaped Gram-positive bacteria, *B. cereus*. The excellent specificity of the *E. coli* sensor was borne from the synergistic specificity effect of the surface PIP and integration of the PBA into the PANI matrix. The PIP captures the pathogen based on the size and shape of the cavity in the polymer network. The PBA captures the pathogen based on the covalent interactions of liposaccharide with boronic acid. Only Gram-negative bacteria have the liposaccharide cell wall structural feature.

With a low LOD of 8.7 ± 0.5 cfu/ml, the developed PIP@PBA/PANI@CNT/CNC sensor hold promise as an inexpensive, miniaturized and versatile platform for onsite monitoring of *E. coli* and other pathogens in various matrices. The PIP sensor demonstrates promise and could be further developed for use in food safety, biomedical and environmental monitoring.

ACKNOWLEDGEMENTS

Mugo research group acknowledges funding from, the Natural Sciences and Engineering Research Council of Canada (NSERC) and Macewan University Research Office.

ORCID

Samuel M. Mugo https://orcid.org/0000-0002-0015-1947

REFERENCES

Ahmed, A., Rushworth, J. V., Wright, J. D., & Millner, P. A. (2013). Novel impedimetric immunosensor for detection of pathogenic bacteria *Streptococcus pyogenes* in Human Saliva. *Analytical Chemistry*, *85*, 12118–12125.

Ajish, J. K., Ajish Kumar, K. S., Ruhela, A., Subramanian, M., Ballal, A. D., & Kumar, M. (2018). AIE based fluorescent self assembled glycoacrylamides for *E. coli* detection and cell imaging. *Sensors & Actuators B. Chemical*, *255*, 1726–1734.

Alzaid, M., Roth, J., Wang, Y., Almutairi, E., Brown, S. L., Dumitrică, T., … Hobbie, E. K. (2017). Enhancing the elasticity of ultrathin single-wall carbon nanotube films with colloidal nanocrystals. *Langmuir*, *33*, 7889–7895.

Blount, Z. D. (2015). The unexhausted potential of *E. coli*. Blount. *eLife*, *4*, e05826.

Brosel-Oliu, S., Abramova, N., Uria, N., & Bratov, A. (2019). Impedimetric transducers based on interdigitated electrode arrays for bacterial detection – A review. *Analytical Chimica Acta*, *1088*, 1–19.

Butina, K., Loffler, S., Rhen, M., & Richter-Dahlfors, A. (2019). Electrochemical sensing of bacteria via secreted redox active compounds using conducting polymers. *Sensors and Actuators B: Chemical*, *297*, 126703.

Dhanjai, Yu, N., & Mugo, S. M. (2019). A flexible-imprinted capacitive sensor for rapid detection of adrenaline. *Talanta*, *204*, 602–606.

Ghaemi, F., Abdullah, L. C., Kargarzadeh, H., Abdi, M. M., Azli, N. F. W. M., & Abbasian, M. (2018). Comparative study of the electrochemical, biomedical, and thermal properties of natural and synthetic nanomaterials. *Nanoscale Research Letters*, *13*, 112.

Golabi, M., Padiolleau, L., Chen, X., Jafari, M. J., Sheikzadeh, E., Turner, A. P. F., … Beni, V. (2016). Doping polypyrrole films with 4-N-Pentylphenylboronic acid to enhance affinity towards bacteria and dopamine. *PLoS ONE*, *11*(11), e0166548. https://doi.org/10.1371/journal.pone.0166548

Gupta, A., Bhardwaj, S. K., Sharma, A. L., Kim, K.-H., & Deep, A. (2019). Development of an advanced electrochemical biosensing platform for *E. coli* using hybrid metal-organic framework/polyaniline composite. *Environmental Research*, *171*, 395–402.

Harris, L. G., Foster, S. J., & Richards, R. G. (2002). An introduction to *Staphylococcus aureus*, and techniques for identifying and quantifying *S. aureus* adhesins in relation to adhesion to biomaterials: Review. *European Cells & Materials*, *4*, 39–60.

Health Canada (2013). *Guidelines for Canadian Drinking Water Quality*. Retrieved from https://www.canada.ca/en/health-canada/services/publications/healthy-living/guidelines-canadian-drinking-water-quality-guideline-technical-document-escherichia-coli.html

Health Canada (2013). *Guidelines for Canadian Recreational Water Quality*. Retrieved from https://www.canada.ca/en/health-canada/services/publications/healthy-living/guidelines-canadian-recreational-water-quality-third-edition/guidelines-canadian-recreational-water-quality-third-edition-page-9.html

Idil, N., Hedstrom, M., Denizli, A., & Mattiasson, B. (2017). Whole cell based microcontact imprinted capacitive biosensor for the detection of *Escherichia coli*. *Biosensors Bioelectronics*, *87*, 807–815.

Isık, P., Neslihan, I., Monireh, B., Erkut, Y., Bo, M., & Adil, D. (2017). Microcontact imprinted plasmonic nanosensors: Powerful tools in the detection of Salmonella paratyphi. *Sensors*, *17*, 1375.

Li, F., & Kosel, J. (2014). An efficient biosensor made of an electromagnetic trap and a magneto-resistive sensor. *Biosensors Bioelectronics*, *59*, 145–150.

Li, M., Zhu, W., Marken, F., & James, T. D. (2015). Electrochemical sensing using boronic acids. *Chemical Communications*, *51*, 14562.

Liu, J. T., Settu, K., Tsai, J.-Z., & Chen, C. J. (2015). Impedance sensor for rapid enumeration of *E. coli* in milk samples. *Electrochimica Acta*, *182*, 89–95.

Ma, Y., Cheung, W., Wei, D., Bogozi, A., Chiu, P. L., Wang, L., … He, H. (2008). Improved conductivity of carbon nanotube networks by in situ polymerization of a thin skin of conducting polymer. *ACS Nano*, *2*, 1197–1204.

Mandal, P. K., Biswas, A. K., Choi, K., & Pal, U. K. (2011). Methods for rapid detection of foodborne pathogens: An overview. *American Journal of Food Technology*, *6*, 87–102.

Nemoto, J., Saito, T., Isogai, A., & Isogai, A. (2015). Simple freeze-drying procedure for producing nanocellulose aerogel-containing, high-performance air filters. *ACS Applied Materials & Interfaces*, *7*, 19809–19815.

Plawsky, J. L., Kim, J. K., & Schubert, E. F. (2009). Engineered nanoporous and nanostructured films. *Materials Today*, *12*, 36–45.

Poller, A. M., Spieker, E., Lieberzeit, P. A., & Preininger, C. (2017). Surface imprints: Advantageous application of ready-2-use materials for bacterial quartz-crystal microbalance sensors. *ACS Applied Materials & Interfaces*, *9*, 1129–1135.

Rengaraj, S., Cruz-Izquierdo, Á., Scott, J. L., & Di Lorenzo, M. (2018). Impedimetric paper-based biosensor for the detection of bacterial contamination in water. *Sensors & Actuators B. Chemical*, *265*, 50–58.

Shen, X., Bonde, J. S., Kamra, T., Bulow, L., Leo, J. C., Linke, D., & Ye, L. (2014). Bacterial imprinting at Pickering emulsion interfaces. *Angewandte Chemie*, *53*, 10687–10690.

Wu, W. H., Li, M., Wang, Y., Ouyang, H.-Q., Wang, L., Li, C.-X., … Lu, J.-X. (2012). Aptasensors for rapid detection of *Escherichia coli* O157:H7 and *Salmonella typhimurium*. *Nanoscale Research Letters*, *7*, 658.

Zhang, J., Oueslati, R., Cheng, C., Zhao, L., Chen, J., Almeida, R., & Wu, J. (2018). Rapid, highly sensitive detection of Gram-negative bacteria with lipopolysaccharide based disposable aptasensor. *Biosensors Bioelectronics*, *112*, 48–53.

Zhang, S., Sun, G., He, Y., Fu, R., Gu, Y., & Chen, S. (2017). Preparation, characterization, and electrochromic properties of nanocellulose based polyaniline nanocomposite films. *ACS Applied Materials & Interfaces*, *9*, 16426–16434.

Zhao, Y., Wang, H., Zhang, P., Sun, C., Wang, X., Wang, X., … Zhou, L. (2016). Rapid multiplex detection of 10 foodborne pathogens with an up-converting phosphor technology-based 10-channel lateral flow assay. *Scientific Reports*, *6*, 21342.

How to cite this article: Mugo SM, Lu W, Dhanjai D. A pathogen imprinted hybrid polymer capacitive sensor for selective *Escherichia coli* detection. *Med Devices Sens*. 2020;3:e10071. https://doi.org/10.1002/mds3.10071